Si_xSb_2Te materials with stable phase for phase change random access memory applications

Yifeng Gu,[1,2,a)] Sannian Song,[1,a)] Zhitang Song,[1] Yan Cheng,[1] Xiaofeng Du,[1] Bo Liu,[1] and Songlin Feng[1]
[1]*State Key Laboratory of Functional Materials for Informatics, Laboratory of Nanotechnology, Shanghai Institute of Micro-system and Information Technology, Chinese Academy of Sciences, Shanghai 200050 China*
[2]*Graduate School of the Chinese Academy of Sciences, Beijing 100049, China*

(Received 18 November 2011; accepted 14 February 2012; published online 15 March 2012)

The physical and electrical properties of Si_xSb_2Te system materials with various Si contents have been systemically studied with the aim of finding the most suitable composition for the phase change random access memory (PCRAM) applications. Si_xSb_2Te shows better thermal stability than $Ge_2Sb_2Te_5$ due to no Te separation under high annealing temperatures. The increase of Si content can enhance the data retention ability of Si_xSb_2Te materials. When the value of x is larger than 0.44, the 10-year data retention temperature for Si_xSb_2Te will exceed 110 °C, which meets the long-term data retention requirement. Furthermore, Si-rich Si_xSb_2Te materials exhibit the improvement on thickness change after annealing compared with $Ge_2Sb_2Te_5$. In addition, the PCRAM devices based on Si_xSb_2Te ($x = 0.31, 0.44$) were fabricated and the electrical operations were carried out. Both of them show the outstanding performances with long-term operations. [http://dx.doi.org/10.1063/1.3693557]

I. INTRODUCTION

Phase-change material is solid characterized by an unconventional combination of properties. On the one hand, it is used extensively in rewritable optical storage media due to the significantly different optical properties between the amorphous and crystalline phases and the ability of being rapidly switched between two phases.[1] On the other hand, it is also considered as one of the most promising candidates for next-generation non-volatile solid-state memory due to its outstanding performances, such as nonvolatility, high scalability, high speed, low power, low cost, and compatibility with complementary metal-oxide semiconductor (CMOS) process.[2–6]

The common phase-change materials applied in phase change random access memory (PCRAM) are chalcogenide alloys. Among these, Te based materials show a pronounced change of electrical properties between amorphous and crystalline phase, and the materials based on Sb can transform between the two phases with considerably rapid speed. In the past few years, various material systems have been investigated to look for the suitable phase-change materials. GeTe-Sb_2Te_3 pseudobinary alloys were studied widely.[7] Sb_2Te_3 displays a fast phase change speed while GeTe shows a good thermal stability. Thus, the ternary composition $Ge_2Sb_2Te_5$ was found out and widely applied in PCRAM devices due to its outstanding performances including a high speed for phase change transformation, a good thermal stability, and a large magnitude of endurance.[8–11] Furthermore, phase-change materials with the element substitution in Ge-Sb-Te system were also investigated in order to improve overall performances. Si-Sb-Te phase-change materials with higher resistances need lower power consumption to be an induced phase transition.[12] Displacing Ge with Sn or Sb with Bi leads to a higher crystallization speed.[13,14] In addition, Se doped Ge-Sb-Se materials were fabricated to improve the storage density with multi-level resistant states.[15]

Sb-Te series materials possess high programming speed due to their growth dominated crystallization mechanism.[16,17] According to the binary phase diagram of Sb-Te, Sb_2Te_3, and Sb_2Te are stable phases in their crystalline states. Compared with Sb_2Te_3, Sb_2Te has a higher crystallization temperature resulting in a better thermal stability but also with high phase transition speed. Hence, considering programming speed in the PCRAM devices, phase-stable property and thermal stability, Sb_2Te is the most suitable composition selected from Sb-Te alloys. However, pure Sb_2Te cannot reach the requirement of high temperature data retention in the PCRAM applications. So our study is mainly focused on the physical and electrical performances by adding the Si atom into Sb_2Te material. The influence of Si dose will be discussed in detail so as to find the best composition for the PCRAM applications.

II. EXPERIMENTAL DETAILS

Si doped Sb_2Te films have been deposited by co-sputtering Si and Sb_2Te targets on SiO_2/Si (100) substrates at room temperature, and $Ge_2Sb_2Te_5$ film was deposited by the $Ge_2Sb_2Te_5$ alloy target. The background pressure and Ar gas pressure were 2.0×10^{-4} and 0.18 Pa, respectively. The thickness of the films was about 150 nm measured by cross-sectional scanning electron microscope (SEM). Compositions of the films were determined by means of energy dispersive spectroscopy (EDS). The films for EDS measurement were deposited on Al foil in order to avoid the

[a)]Authors to whom correspondence should be addressed. Electronic addresses: yifenggu@mail.sim.ac.cn and songsannian@mail.sim.ac.cn. Fax: +86-21-62134404.

influence of Si atoms in the SiO_2/Si substrates. *In situ* temperature dependent sheet resistance (*in situ* R-T) measurements for all the compositions of Si_xSb_2Te and $Ge_2Sb_2Te_5$ were performed in a vacuum chamber with a heating rate of 20 °C/min. These measurements were carried out in discrete temperature with the step of 2 °C. The following *in situ* R-T measurement for $Si_{0.44}Sb_2Te$ with different heating rates also employed the same method. The activation energy for crystallization E_a of the films was calculated by Kissinger's analysis. Isothermal change of sheet resistance was utilized to characterize the data retention of amorphous films. The E_a values were also achieved by the Arrhenius equation. Comparing the E_a results of these two calculation methods, it can prove the accuracy of them. The films were annealed in N_2 atmosphere at various temperatures for 1 min for the X-ray diffraction (XRD) measurement. XRD patterns were taken in the 2θ range of 20°–65° using Cu/K-α radiation ($\lambda = 1.54056$ Å) with a scanning step of 0.02°. Bright filed images and their corresponding selected area electron diffraction (SAED) patterns in transmission electron microscopy (TEM) equipped with heating holder were used to characterize the effects of annealing on phase change materials. The crystallization of Si doped Sb_2Te films have been studied by observation of their microstructure and morphology changes during *in situ* heating process in TEM. The films were deposited on the TEM sample supporting grids coated with carbon film. The thickness of the phase-change materials for TEM measurement was about 40 nm. The Si_xSb_2Te film thickness changes upon crystallization were achieved from X-ray reflectometry (XRR) measurement depositing the film on the Si substrate with the thickness about 40 nm. T-shaped PCRAM cells based on Si_xSb_2Te materials were fabricated by 0.18 μm complementary metal-oxide-semiconductor (CMOS) technology. They were employed to test the electrically induced phase change performance of Si_xSb_2Te materials. The diameter of the bottom W electrode was 260 nm. Si_xSb_2Te films were deposited on the W electrode with the thickness about 100 nm. TiN (20 nm) and Al (300 nm) were applied as the top electrodes. The resistance-voltage (R-V) and endurance measurements were monitored by using a Keithley 2600 m and AWG5002B.

III. RESULTS AND DISCUSSION

A. Temperature dependence of sheet resistance

Figure 1 displays the resistance as a function of temperature with various compositions of Si_xSb_2Te compared with $Ge_2Sb_2Te_5$ using the heating rate of 20 °C/min. As annealing temperature increases, a continuous decrease of resistance for all the films is observed before reaching their respective crystallization temperature (T_c). An abrupt drop of resistance occurs when the temperature reaches T_c s for $Ge_2Sb_2Te_5$ and Si_xSb_2Te films. The decrease of resistance with temperature increase before the sudden drop indicates a semiconductor-like behavior.

The temperature dependence for the resistance of semiconductor can be expressed by[18]

$$\rho = \rho_0 \exp(-E_\sigma/kT),$$

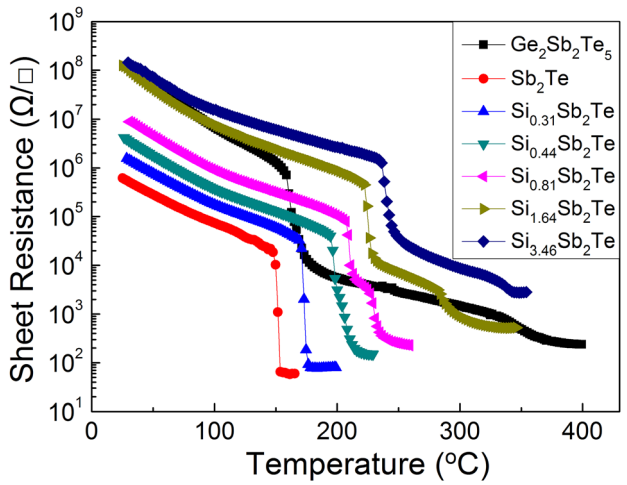

FIG. 1. (Color online) Resistance as a function of temperature with various compositions of Si_xSb_2Te compared with $Ge_2Sb_2Te_5$ (heating rate $dT/dt = 20$ K/min).

where ρ_0 is a pre-exponential factor and E_σ is the activation energy for electrical conduction. Using the above expression (shown in Fig. 2), the activation energy for electrical conduction E_σ of $Ge_2Sb_2Te_5$, Sb_2Te, $Si_{0.31}Sb_2Te$, $Si_{0.44}Sb_2Te$, $Si_{0.81}Sb_2Te$, and $Si_{1.64}Sb_2Te$ are ~0.401 eV, ~0.270 eV, ~0.291 eV, ~0.311 eV, ~0.322 eV, and ~0.363 eV, respectively (shown in Table I). Furthermore, the pinning of the Fermi level in the middle of the bandgap ensures that the activation energy for electron transport is given as

$$E_\sigma = E_g/2 + \Delta E,$$

where $E_g/2$ is the distance from the Fermi level to the conduction band and ΔE is the depth of the trap states. Due to intrinsic conduction in which the number of electrons and holes with the equal amount, the Fermi level will be situated at the middle of the bandgap and the activation energy for electron transport is given simply as half the bandgap energy. Thus according to the values of E_σ, we can estimate the optical gaps of amorphous $Ge_2Sb_2Te_5$, Sb_2Te, $Si_{0.31}Sb_2Te$,

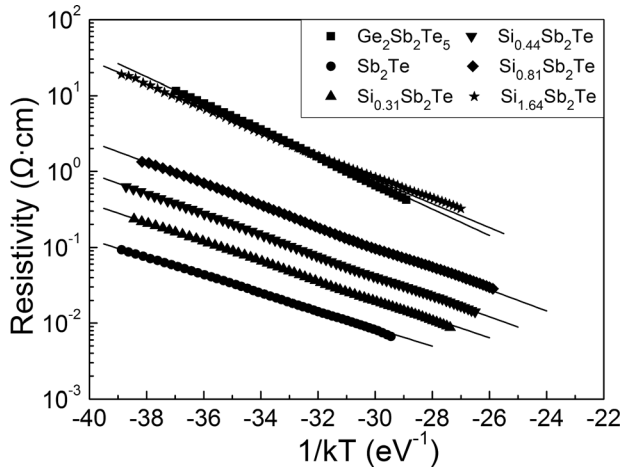

FIG. 2. Fitting curves for calculating electrical activation energies of $Ge_2Sb_2Te_5$, Sb_2Te, and Si_xSb_2Te materials.

TABLE I. Measured crystallization temperatures and calculated activation energies for electrical conduction, crystallization activation energies, and 10-year data retention temperatures for $Ge_2Sb_2Te_5$ and Si_xSb_2Te films.

	T_c (°C)	E_σ (eV)	E_a (eV)	10-year data retention T (°C)
$Ge_2Sb_2Te_5$	160.7	0.401 ± 0.00154	2.866 ± 0.0838	82
Sb_2Te	151.7	0.270 ± 0.00097	...	...
$Si_{0.31}Sb_2Te$	172.9	0.291 ± 0.00116	2.955 ± 0.0491	90.4
$Si_{0.44}Sb_2Te$	198.3	0.311 ± 0.00085	3.018 ± 0.0504	110.9
$Si_{0.81}Sb_2Te$	211	0.322 ± 0.00135	3.326 ± 0.0702	124.3
$Si_{1.64}Sb_2Te$	224.1	0.363 ± 0.00179	3.432 ± 0.0588	136.3
$Si_{3.46}Sb_2Te$	238.3	...	3.560 ± 0.0513	148.4

$Si_{0.44}Sb_2Te$, $Si_{0.81}Sb_2Te$, and $Si_{1.64}Sb_2Te$ to be ~0.802 eV, ~0.540 eV, ~0.582 eV, ~0.622 eV, ~0.644 eV, and ~0.726 eV, respectively. The calculated value of the bandgap for $Ge_2Sb_2Te_5$ is a little larger than the experimental result ~0.7 eV measured by optical spectroscopy.[19] The deviation may derive from the different testing methods and the film thicknesses. Since amorphous Si has a larger bandgap (1.7 eV) compared to amorphous Sb_2Te (~0.540 eV), with doping more Si element, the band gaps of Si_xSb_2Te monotonically will become wider. On the other hand, the band tail of the valence band induced by the localized Te lone pairs or the structural defects along the Te-Te chains in the amorphous phase are supposed to be suppressed or reduced due to the defect saturation effect caused by Si addition.[20,21]

According to Fig. 1, as Si content increases, T_c of Si_xSb_2Te film goes up. Doping with high glass-transition temperature (T_g) such as Ge (T_g = 477°C) added into Sb-Te materials can effectively enhance T_c.[22] Compared with Ge, Si has an even higher T_g (~727 °C), so it also can help increase T_c of the material when doping it into the Sb-Te film. In addition, due to larger electronegativity difference between the Si element and Sb, Te, more Si dopant will

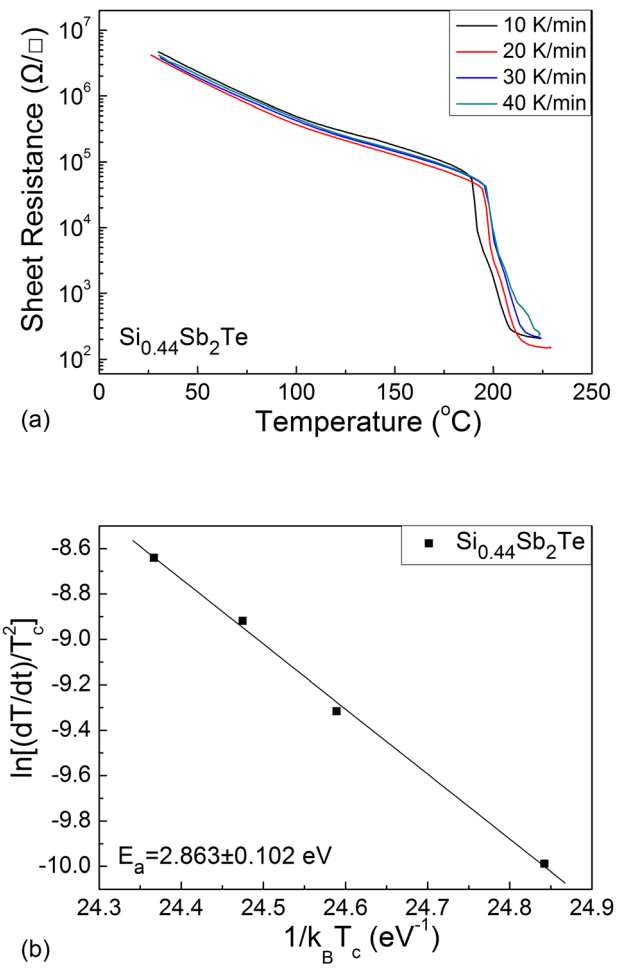

FIG. 3. (Color online) (a) Sheet resistance of $Si_{0.44}Sb_2Te$ film as a function of temperature with various heating rates; (b) corresponding Kissinger's plot for E_a calculation.

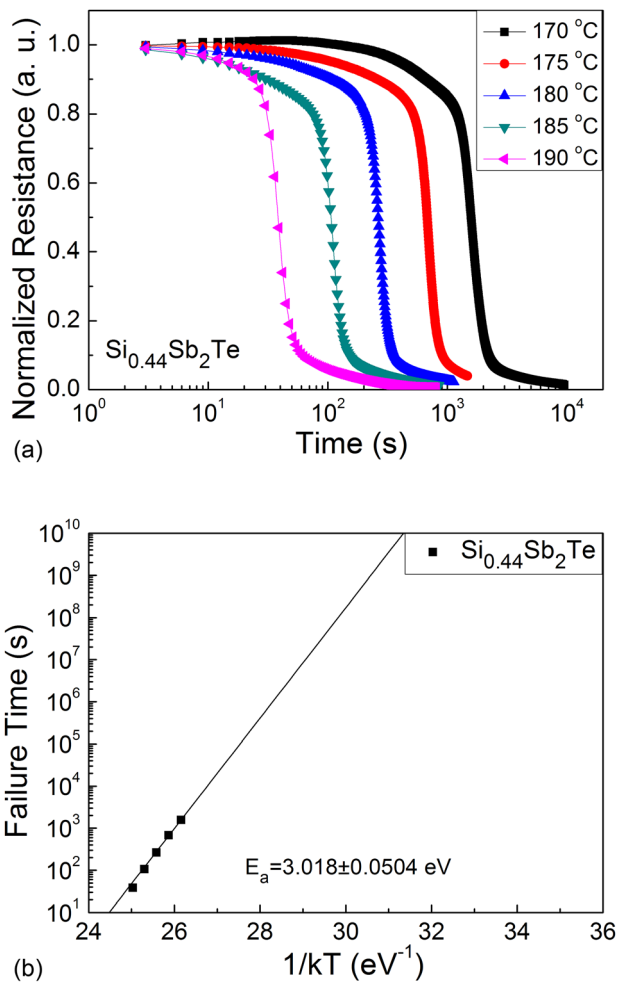

FIG. 4. (Color online) (a) The plots of normalized resistance vs time at different isothermal annealing temperatures for $Si_{0.44}Sb_2Te$ film; (b) corresponding Arrhenius fitting plot of failure time vs reciprocal temperature.

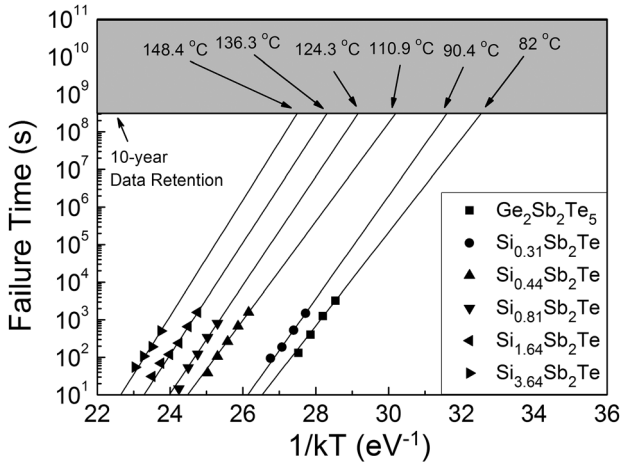

FIG. 5. Arrhenius fitting plots for $Ge_2Sb_2Te_5$ and all compositions of Si_xSb_2Te and the temperatures corresponding to the 10-year data retention marked.

reduce the atomic diffusivity resulting from the introduced covalent bonds, which will reinforce the cohesion of the atom network, leading to the increase of T_c.[23] T_c is identified as the temperature at which the derivative of (dR/dT) reaches the minimum value[10] and Table I lists the measured T_c values of $Ge_2Sb_2Te_5$, Sb_2Te, and Si_xSb_2Te: $Ge_2Sb_2Te_5$ ~160.7 °C, Sb_2Te ~151.7 °C, $Si_{0.31}Sb_2Te$ ~172.9 °C, $Si_{0.44}Sb_2Te$ ~198.3 °C, $Si_{0.81}Sb_2Te$ ~211 °C, $Si_{1.64}Sb_2Te$ ~224.1 °C, and $Si_{3.46}Sb_2Te$ ~238.3 °C. These measured T_c values are a little larger than those we achieved in the previous work.[24] The deviation between these two measurements may result from the different methods of fabricating films. Si_xSb_2Te films were fabricated by the Si target and Sb_2Te alloy target this time, while the films were fabricated by the Si, Sb, and Te target before. Larger T_c may result in the rise of power consumption in the PCRAM SET operation, while a properly high T_c will also help to improve the thermal stability of the amorphous film.

Figure 3(a) shows that higher heating rate results in T_c of $Si_{0.44}Sb_2Te$ film. Kissinger's analysis is applied to relate

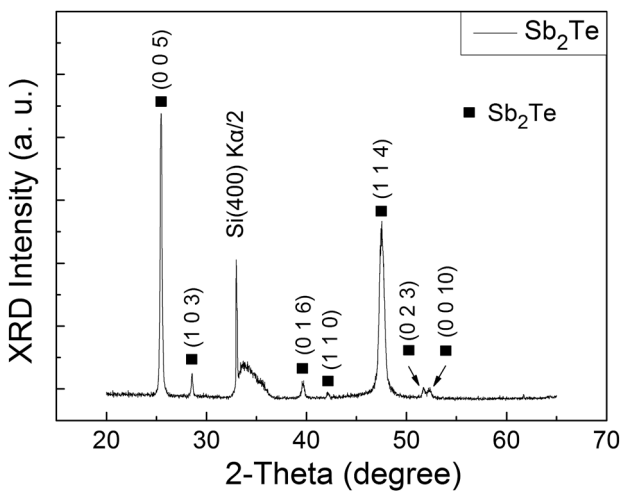

FIG. 6. XRD pattern of annealed Sb_2Te film at 180 °C for 1 min.

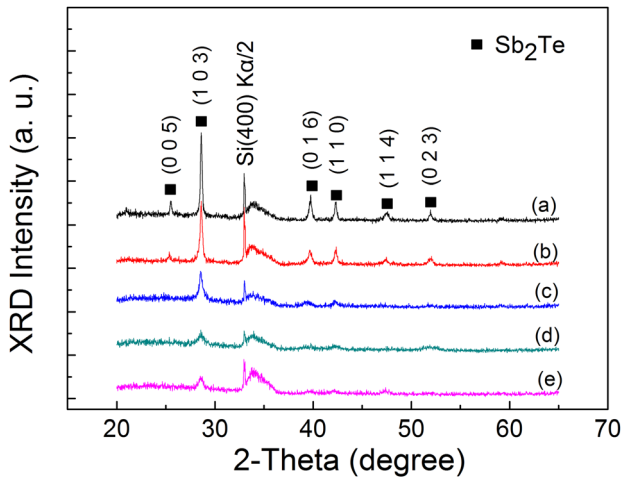

FIG. 7. (Color online) XRD pattern of annealed Si_xSb_2Te films at various temperatures: (a) $Si_{0.31}Sb_2Te$ at 200 °C for 1 min; (b) $Si_{0.44}Sb_2Te$ at 300 °C for 1 min; (c) $Si_{0.81}Sb_2Te$ at 300 °C for 1 min; (d) $Si_{1.64}Sb_2Te$ at 400 °C for 1 min; (e) $Si_{3.46}Sb_2Te$ at 400 °C for 1 min.

T_c, the heating rate dT/dt, and the activation energy for crystallization E_a by the following formula:

$$\ln[(dT/dt)/T_c^2] = C + (E_a/k_BT_c),$$

where C is a constant and k_B is the Boltzmann constant. To determine the accuracy of the calculated E_a of Si_xSb_2Te above, the composition of $Si_{0.44}Sb_2Te$ is taken, for example, by Kissinger's analysis. A plot of $\ln[(dT/dt)/T_c^2]$ against $1/k_BT_c$ yields a straight line with slope E_a (~2.863 ± 0.102 eV) as shown in Fig. 3(b).

Figure 4(a) shows the curves of normalized resistance versus time for $Si_{0.44}Sb_2Te$ film at various annealing temperatures (170 °C, 175 °C, 180 °C, 185 °C, and 190 °C). At higher isothermal annealing temperature, shorter time is required for sheet resistance to fall to half of its initial magnitude, which denotes a faster grain growth process since no obvious incubation period is found for all curves.[6] Figure 4(b) shows the fitting for failure time versus reciprocal temperature $1/k_BT$ by the Arrhenius equation,[25]

$$t = \tau \exp(E_a/k_BT),$$

where t is failure time and τ is a proportional time coefficient. The calculated E_a value using Arrhenius equation is ~3.018 ± 0.0504 eV which is close to the previous one achieved by Kissinger's method ~2.863 ± 0.102 eV. This proves that E_a values achieved in our work are reasonably correct. By using the Arrhenius equation, the E_a results are listed in Table I. On the other hand, the Arrhenius fitting line estimates that $Si_{0.44}Sb_2Te$ has a data retention

TABLE II. Gain size for various compositions of annealed Si_xSb_2Te films corresponding to XRD measurement.

	$Si_{0.31}Sb_2Te$	$Si_{0.44}Sb_2Te$	$Si_{0.81}Sb_2Te$	$Si_{1.64}Sb_2Te$	$Si_{3.46}Sb_2Te$
Grain size (nm)	44.1	31.9	15.2	9.8	6.3

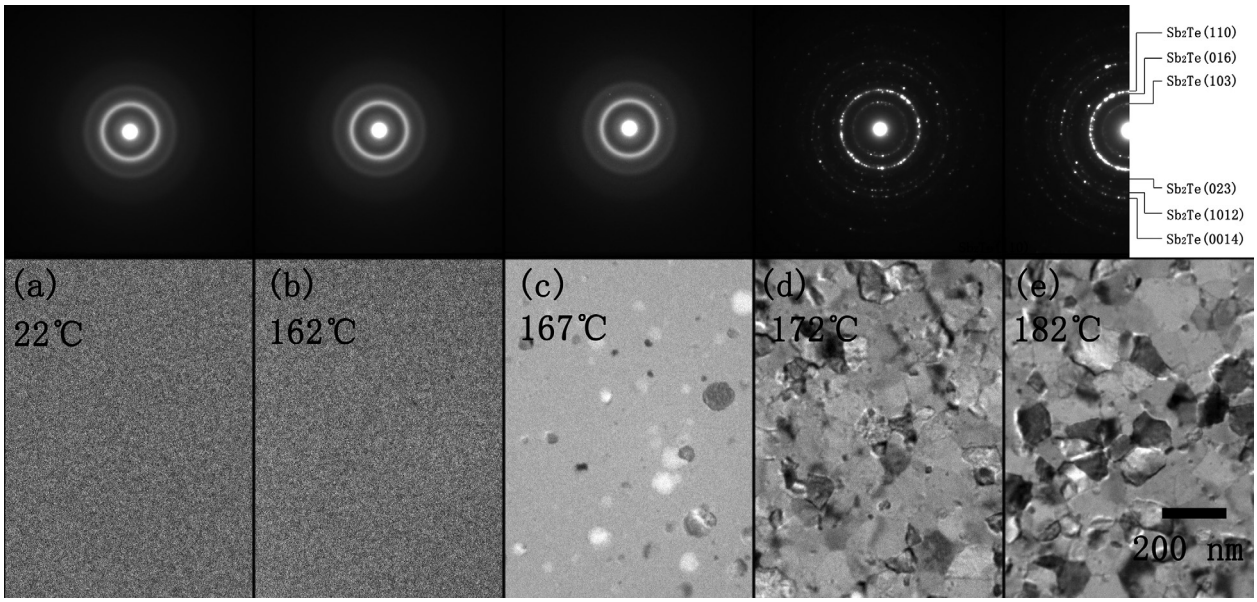

FIG. 8. TEM images and SAED patterns of $Si_{0.31}Sb_2Te$ films with *in situ* heating.

temperature 110.9 °C for 10 years. Furthermore, the data retention temperatures for 10 years of all the compositions of Si_xSb_2Te and $Ge_2Sb_2Te_5$ have been achieved as shown in Fig. 5 and listed in Table I. Data retention has already been considered sufficient to meet the long-term data storage requirement of automotive electronics, at least 120 °C for 10 years.[26]

B. Crystalline structures of Si_xSb_2Te films

Figures 6 and 7 show the XRD patterns of Sb_2Te and Si_xSb_2Te after annealing at different temperatures for 1 min: Sb_2Te at 180 °C, $Si_{0.31}Sb_2Te$ at 200 °C, $Si_{0.44}Sb_2Te$ and $Si_{0.81}Sb_2Te$ at 300 °C, $Si_{1.64}Sb_2Te$ and $Si_{3.46}Sb_2Te$ at 400 °C, respectively. The peak of Si in the figure denotes Si (400) $K\alpha/2$ which belongs to the substrate. Both in Fig. 6 and Fig. 7, except the Si peak, all the other peaks correspond to Sb_2Te. It shows that with an increase of Si content, there is no change of the major peaks in the patterns. It demonstrates that when Si atoms doped into Sb_2Te, it does not change the lattice structure, which belongs to the δ-phase rhombohedral crystalline structure.[9] Maybe the Si atom only exists among the grains, and does not bond with other atoms (Sb and Te).[27] The role of the Si atom is to improve crystallization temperature and thermal stability of the films. As shown in Fig. 7, the strength of the diffraction peaks decreases with an increase of Si content. The composition with lower dose of Si has a small full width at half maximum (FWHM) value as compared with the higher dose. The crystalline grain size for the various compositions was calculated by means of the Scherrer formula,

$$d = K\lambda/\beta\cos\theta,$$

where d is the size of the grain, K is the constant of Scherrer, λ is X-ray wavelength ($\lambda = 0.154056$ nm), β is FWHM, and θ is angle of diffraction, respectively. The grain size of the

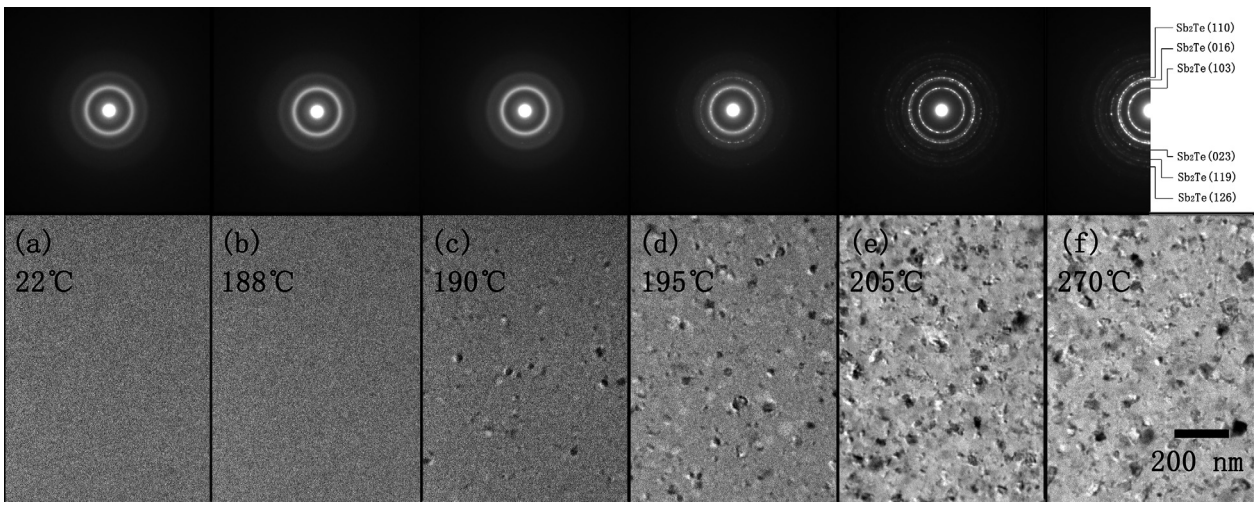

FIG. 9. TEM images and SAED patterns of $Si_{0.44}Sb_2Te$ films with *in situ* heating.

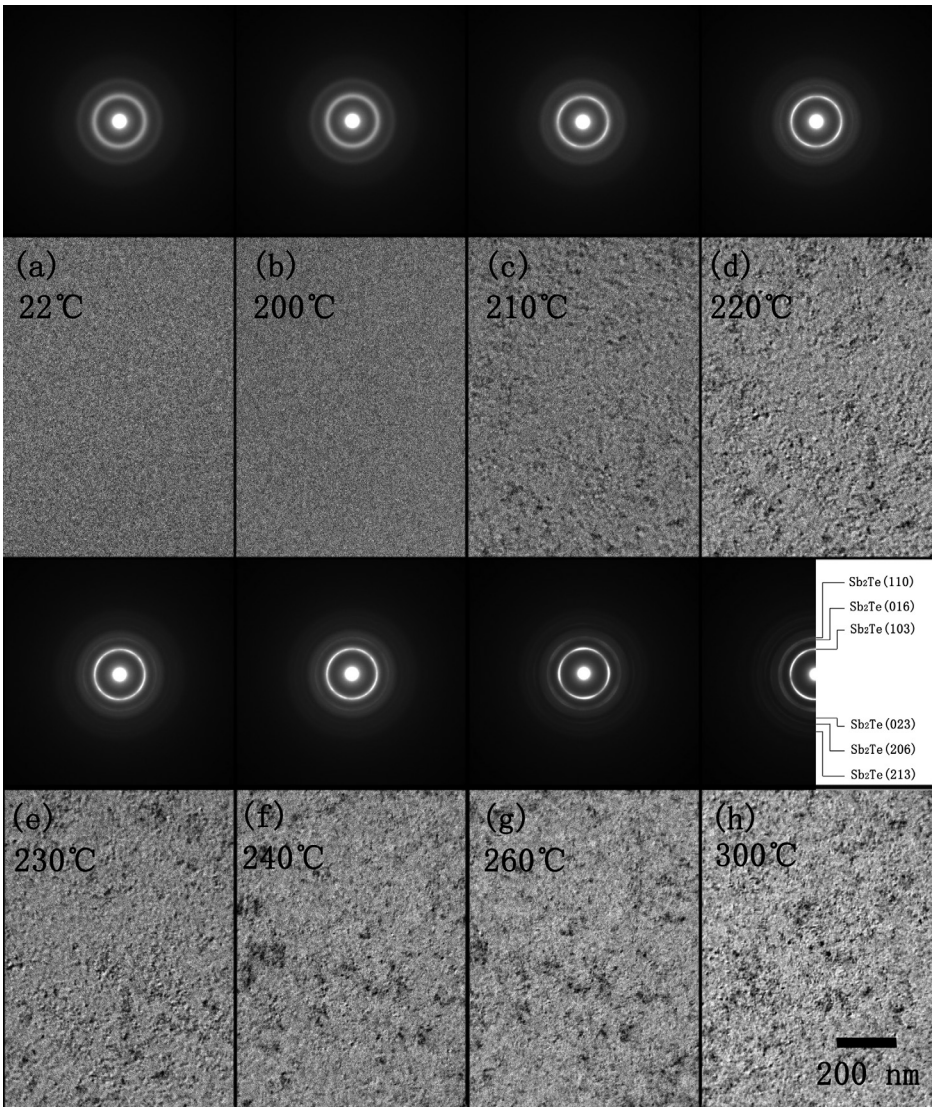

FIG. 10. TEM images and SAED patterns of $Si_{1.64}Sb_2Te$ films with *in situ* heating.

Si_xSb_2Te phase change material decreases with an increase of Si atomic content as shown in Table II. It implies that doping of Si restrains the growth of Sb_2Te grain size.

Figures 8–10 show TEM bright-field images and their corresponding SAED patterns of $Si_{0.31}Sb_2Te$, $Si_{0.44}Sb_2Te$, and $Si_{1.64}Sb_2Te$ films with as-deposited and *in situ* annealed states, respectively. Panel (a) in the three figures all show the TEM bright-field images and their corresponding SAED patterns of the as-deposited samples, revealing that all the samples have the typical amorphous structure. Figures 8(b)–8(e) display TEM images and SAED patterns of the $Si_{0.31}Sb_2Te$ film by *in situ* heating. According to the figure, it shows that the $Si_{0.31}Sb_2Te$ film starts to crystallize when the temperature reaches 167 °C. Similarly, in Figs. 9(b)–9(f) and Figs. 10(b)–10(h), the crystallization temperatures of $Si_{0.44}Sb_2Te$ and $Si_{1.64}Sb_2Te$ films are 190 °C and 210 °C, respectively. Through indexing of the last SAED patterns of the three figures, crystallized Si doped Sb_2Te films can be assigned to pure Sb_2Te with the rhombohedral structure. On the other hand, with an increase of Si atomic content, the grains become smaller in the crystalline state as shown in the TEM images. From Fig. 8, it denotes that growth is the dominant crystallizing type for $Si_{0.31}Sb_2Te$. But as Si content increases, the growth of grains are restrained, so there is a tendency that crystallizing type changes from growth domination to nucleation domination is shown in Figs. 9 and 10.

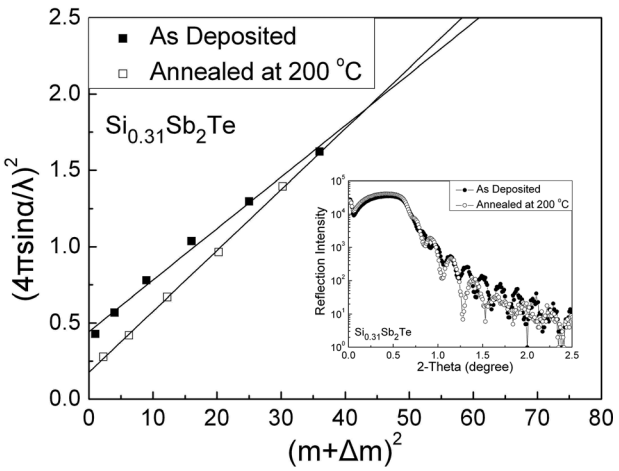

FIG. 11. XRR measurement of $Si_{0.31}Sb_2Te$ film in the as-deposited and annealed states. The inset is the plot of amendatory Bragg fitting curve.

TABLE III. The thickness reduction between amorphous and crystalline phase for $Ge_2Sb_2Te_5$ and Si_xSb_2Te films.

	$Ge_2Sb_2Te_5$	$Si_{0.31}Sb_2Te$	$Si_{0.44}Sb_2Te$	$Si_{0.81}Sb_2Te$	$Si_{1.64}Sb_2Te$	$Si_{3.46}Sb_2Te$
Film thickness reduction (%)	8.2	8.01	6.88	4.52	1.62	0.51

It implies that Si atoms do not enter into the crystal lattice of Sb_2Te, and only exist as amorphous state among grains, which is similar with Si doped Sb_2Te_3 materials.[27] Due to this, the influence of Si atoms represents two points. One is to restrain the growth of Sb_2Te grains and the other is to form a cluster. However, it does not change the crystalline structure of the material corresponding to the XRD measurement.

C. Film thickness and density reduction upon crystallization

Phase transition from amorphous to crystalline state induces stress in the film which results in an observable thickness change. XRR measurement was employed and the precise values were achieved by means of a mandatory Bragg equation[28]

$$q_m^2 = 2\delta(4\pi/\lambda)^2 + (m + \Delta m)^2(2\pi/d)^2,$$

where m is reflection degree, λ is the wavelength of the X-ray ($\lambda = 0.154056$ nm), $q_m = 4\pi \sin\alpha/\lambda$ (α is the angle corresponding to the maximum or the minimum of the reflection curve in the m degree), δ is coefficient of scattering, and d is the thickness of the film. Si_xSb_2Te films were prepared in different annealing temperatures to ensure the complete crystallization and avoid the volatility of the materials. Figure 11 shows the XRR measurement of $Si_{0.31}Sb_2Te$ film in the as-deposited and crystalline states and the modified Bragg fitting curve. Table III lists the calculated values of thickness change for all compositions of Si_xSb_2Te and the reported value of $Ge_2Sb_2Te_5$.[29] Comparing the thickness reduction value of $Ge_2Sb_2Te_5$, Si_xSb_2Te films have lower values, the maximum for $Si_{0.31}Sb_2Te \sim 8.01\%$ and the minimum for $Si_{3.46}Sb_2Te$ $\sim 0.51\%$, which implies that the stress accompanying to the phase transition is smaller for Si_xSb_2Te materials than that of $Ge_2Sb_2Te_5$. Te segregation to the boundary and surface at high annealing temperature is responsible for inducing an extra post-transition stress release.[30] Thus, reducing Te content will be helpful to lower the stress amplitude during phase transition. In addition, as Si content increases, the thickness change of Si_xSb_2Te will be further restrained.

D. Electrical properties of the PCRAM memory cell based on Si_xSb_2Te

PCRAM cells based on $Si_{0.31}Sb_2Te$ and $Si_{0.44}Sb_2Te$ materials with a heating electrode of 260 nm in diameter were fabricated and characterized. These two compositions possess better 10-year data retention ability than $Ge_2Sb_2Te_5$, but also maintain high phase transition speed. Reversible phase-change process has been observed by SET and RESET operations. Figure 12 shows current-voltage (I–V) characteristic curves for the fabricated PCRAM cells for $Si_{0.31}Sb_2Te$ and $Si_{0.44}Sb_2Te$. The threshold current (I_{th}) and threshold voltage (V_{th})of $Si_{0.31}Sb_2Te$ are 9 μA and 1.27 V, while 12 μA and 1.44 V for $Si_{0.44}Sb_2Te$. During resistance-voltage (R-V) measurement, SET-RESET operation with the pulse width of 100 ns was carried out as shown in Fig. 13. The resistance ratio of the high-resistance state ($\sim 2 \times 10^6$ Ω) and low-resistance state ($\sim 5 \times 10^3$ Ω) is ~100 for $Si_{0.31}Sb_2Te$, and for $Si_{0.44}Sb_2Te$ the resistance ratio of the high-resistance state ($\sim 4 \times 10^6$ Ω) and low-resistance state ($\sim 6 \times 10^3$ Ω) is also ~100. $Si_{0.31}Sb_2Te$ memory cell needs 0.8 V to transform from RESET state to SET state and 2.9 V voltage value is provided to induce the cell to amorphize. Nevertheless, SET operating voltage is 1.0 V and RESET operating voltage is 3.2 V for $Si_{0.44}Sb_2Te$. The endurance performance of

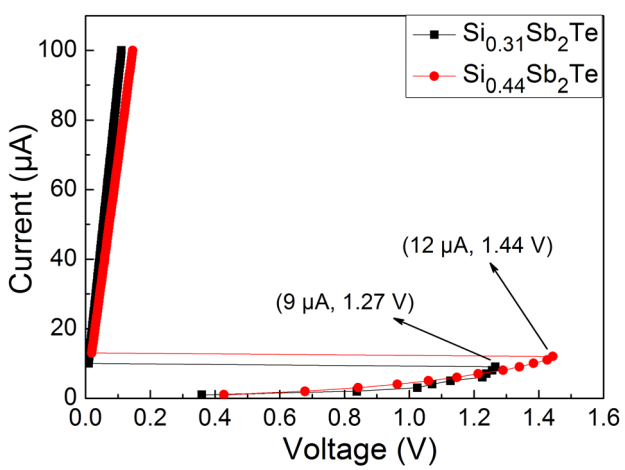

FIG. 12. (Color online) I–V characteristic curves of PCRAM cells based on $Si_{0.31}Sb_2Te$ and $Si_{0.44}Sb_2Te$.

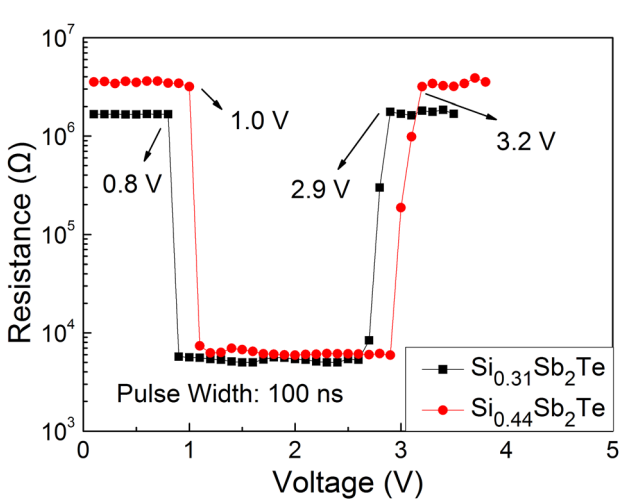

FIG. 13. (Color online) SET-RESET window characteristic curves of PCRAM cells based on $Si_{0.31}Sb_2Te$ and $Si_{0.44}Sb_2Te$ with the voltage pulse width of 100 ns.

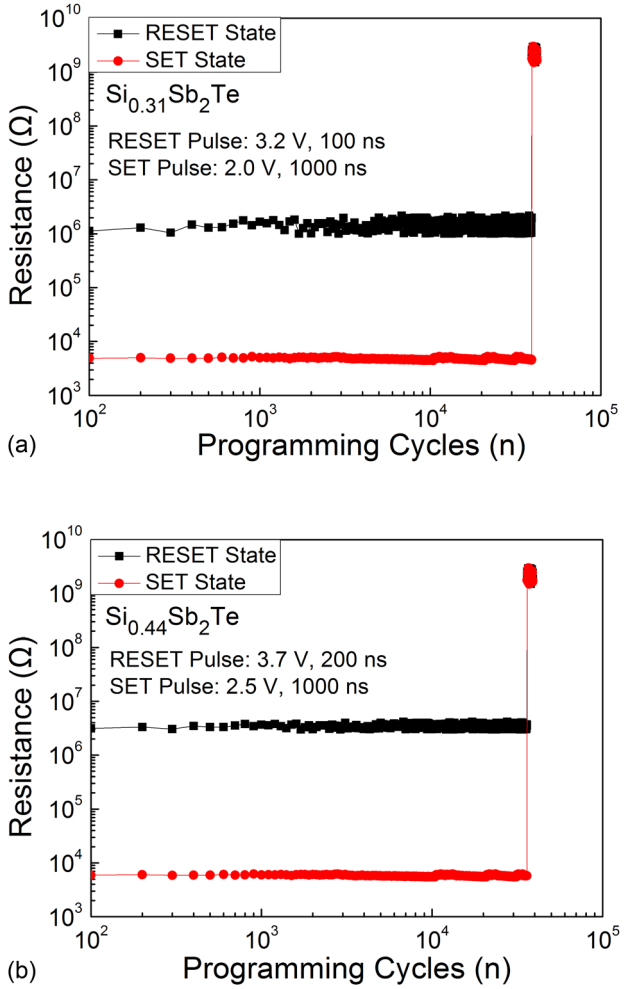

FIG. 14. (Color online) Endurance characteristic curves of PCRAM cells based on $Si_{0.31}Sb_2Te$ and $Si_{0.44}Sb_2Te$: (a) $Si_{0.31}Sb_2Te$ with RESET pulse of 3.2 V, 100 ns and SET pulse of 2.0 V 1000 ns; (b) $Si_{0.44}Sb_2Te$ with RESET pulse of 3.7 V, 200 ns and SET pulse of 2.5 V 1000 ns.

a cell, respectively, based on $Si_{0.31}Sb_2Te$ and $Si_{0.44}Sb_2Te$ materials is shown in Fig. 14. The $Si_{0.31}Sb_2Te$ memory cell can reach $\sim 3.9 \times 10^4$ cycles for reversible phase change transition and the value for $Si_{0.31}Sb_2Te$ memory cell is $\sim 3.6 \times 10^4$. After their respective extreme cycles, their resistances will become disordered.

IV. CONCLUSION

Various compositions of Si_xSb_2Te films have been fabricated to study the thermal properties and crystalline structures. According to the results, Si_xSb_2Te materials can maintain the stable phase after annealing at high temperature. Increasing the Si content will enhance the T_c and improve the thermal stability of the materials. Regardless of the dose of Si in the films, the crystalline structures are all based on the Sb_2Te structure. Si atoms only exist among the grains, and do not bond with other atoms (Sb and Te). Furthermore, the thickness reduction during phase transition becomes weak with the increase of Si content. PCRAM cells based on $Si_{0.31}Sb_2Te$ and $Si_{0.44}Sb_2Te$ have been prepared in order to characterize the electrical performances. They both show stable and long-term reversible operations.

ACKNOWLEDGMENTS

This work is supported by the National Integrate Circuit Research Program of China (2009ZX02023-003), National Key Basic Research Program of China (2010CB934300, 2011CBA00602, 2011CB932800), National Natural Science Foundation of China (60906004, 60906003, 61006087, 61076121), Science and Technology Council of Shanghai (1052nm07000).

[1]M. Wuttig and N. Yamada, Nature Mater. **6**, 824 (2007).
[2]S. L. Cho, J. H. Yi, Y. H. Ha, B. J. Kuh, C. M. Lee, J. H. Park, S. D. Nam, H. Horii, B. K. Cho, K. C. Ryoo, S. O. Park, H. S. Kim, U. Chung, J. T. Moon, and B. I. Ryu, Symposium on VLSI Technology Digest of Technical, 2005, p. 96.
[3]S. J. Ahn, Y. N. Hwang, Y. J. Song, S. H. Lee, S. Y. Lee, J. H. Park, C. W. Jeong, K. C. Ryoo, J. M. Shin, Y. Fai, J. H. Oh, G. H. Koh, G. T. Jeong, S. H. Joo, S. H. Choi, Y. H. Son, J. C. Shin, Y. T. Kim, H. S. Jeong, and K. Kim, Symposium on VLSI Technology Digest of Technical, 2005, p. 98.
[4]M. Wuttig and C. Steimer, Appl. Phys. A **87**, 411 (2007).
[5]A. Pirovano, A. Lacaita, A. Benvenuti, F. Pellizer, S. Hudgens, and R. Bez, *IEEE P. Int. Electron. Devices Meeting*, 2003, p. 699.
[6]G. Muller, T. Happ, M. Kund, G. Y. Lee, N. Nagel, and R. Sezi, *IEEE P. Int. Electron. Devices Meeting*, 2004, p. 567.
[7]N. Yamada, E. Ohno, K. Nishiuchi, N. Akahira, and M. Takao, J. Appl. Phys. **69**, 2849 (1991).
[8]S. R. Ovshinsky, Phys. Rev. Lett. **21**, 1450 (1968).
[9]T. C. Chong, L. P. Shi, R. Zhao, P. K. Tan, J. M. Li, H. K. Lee, and X. S. Miao, Appl. Phys. Lett. **88**, 122114 (2006).
[10]I. Friedrich, V. Weidenhof, W. Njoroge, P. Franz, and M. Wuttig, J. Appl. Phys. **87**, 4130 (2000).
[11]N. Takaura, M. Terao, K. Kurotsuchi, T. Yamauchi, O. Tonomura, Y. Hanaoka, R. Takemura, K. Osada, T. Kawahara, and H. Matsuoka, *Tech. Dig. Int. Electron Devices Meeting*, 2003, p. 897.
[12]B. Qiao, J. Feng, Y. Lai, Y. Cai, Y. Lin, T. Tang, B. Cai, and B. Chen, Semicond. Sci. Technol. **21**, 1073 (2006).
[13]W. D. Song, L. P. Shi, X. S. Miao, and T. C. Chong, Appl. Phys. Lett. **90**, 091904 (2007).
[14]S. F. Chen, J. K. Chen, and T. P. Chen, Mater. Sci. Technol. **24**, 501 (2008).
[15]Y. F. Gu, Z. T. Song, T. Zhang, B. Liu, and S. L. Feng, Solid-State Electron. **54**, 443 (2010).
[16]R. Pandian, B. J. Kooiand, and J. Th. M. De Hosson, J. Appl. Phys. **101**, 053529 (2007).
[17]R. Pandian, B. J. Kooiand, and J. Th. M. De Hosson, J. Appl. Phys. **100**, 123511 (2006).
[18]K. Chung, D. Wamwangi, M. Woda, M. Wuttig, and W. Bensch, J. Appl. Phys. **103**, 083523 (2008).
[19]B. Lee, J. R. Abelson, S. G. Sishop, D. Kang, B. Cheong, and K. Kim, J. Appl. Phys. **97**, 093509 (2005).
[20]Y. Zhang, J. Feng, Z. Zhang, B. Cai, Y. Lin, T. Tang, and B. Chen, Appl. Surf. Sci. **254**, 5602 (2008).
[21]A. Pirovano, A. L. Lacaita, A. Benvenuti, F. Pellizzer, and R. Bez, IEEE Trans. Electron Devices **51**, 452 (2004).
[22]B. J. Kooi and J. Th. M. De Hosson, J. Appl. Phys. **95**, 4714 (2004).
[23]J. Feng, Z. Zhang, Y. Zhang, B. Cai, Y. Lin, T. Tang, and B. Chen, J. Appl. Phys. **101**, 074502 (2007).
[24]Y. F. Gu, Y. Cheng, S. N. Song, T. Zhang, Z. T. Song, X. Y. Liu, X. F. Du, B. Liu, and S. L. Feng, Scr. Mater. **65**, 622 (2011).
[25]M. H. R. Lankhorst, L. Can Pieterson, M. van Schijindel, B. A. J. Jacobs, and J. C. N. Rijpers, Jpn. J. Appl. Phys. **42**, 863 (2003).
[26]K. F. Kao, C. M. Lee, M. J. Chen, M. J. Tsai, and T. S. Chin, Adv. Mater. **21**, 1695 (2009).
[27]X. L. Li, F. Rao, Z. T. Song, K. Ren, W. L. Liu, and Z. M. Sun, Appl. Surf. Sci. **257**, 4566 (2011).
[28]J. C. Zhang, Y. J. Tang, and W. D. Wu, Laser Part. Beams **19**, 1317 (2007).
[29]W. K. Njoroge, H. W. Woltgens, and M. Wuttig, J. Vac. Sci. Technol. A **20**, 230 (2002).
[30]L. Krusin-Elbaum, C. Cabral, K. N. Chen, M. Copel, D. W. Abraham, J. Bruley, and V. R. Deline, Appl. Phys. Lett. **90**, 141902 (2007).